remote sensing

MDPI

Letter

Exploring the Relationship between Burn Severity Field Data and Very High Resolution GeoEye Images: The Case of the 2011 Evros Wildfire in Greece

Eleni Dragozi [1,*], Ioannis Z. Gitas [1,†], Sofia Bajocco [2,†] and Dimitris G. Stavrakoudis [1,†]

[1] School of Forestry and Natural Environment, Faculty of Agriculture, Forestry and Natural Environment, Aristotle University of Thessaloniki, Thessaloniki 54124, Greece; igitas@for.auth.gr (I.Z.G.); jstavrak@auth.gr (D.G.S.)

[2] Consiglio per la Ricerca in Agricoltura e l'Analisi dell'Economia Agraria, Research Unit for Climatology and Meteorology Applied to Agriculture (CREA-CMA), Rome 00186, Italy; sofia.bajocco@crea.gov.it

* Correspondence: edragozi@for.auth.gr; Tel.: +30-2310-992-688; Fax: +30-2310-992-677

† These authors contributed equally to this work.

Academic Editors: Diofantos Hadjimitsis, Luigi Boschetti, Kyriacos Themistocleous, Parth Sarathi Roy and Prasad S. Thenkabail

Received: 28 March 2016; Accepted: 30 June 2016; Published: 5 July 2016

Abstract: Monitoring post-fire vegetation response using remotely-sensed images is a top priority for post-fire management. This study investigated the potential of very-high-resolution (VHR) GeoEye images on detecting the field-measured burn severity of a forest fire that occurred in Evros (Greece) during summer 2011. To do so, we analysed the role of topographic conditions and burn severity, as measured in the field immediately after the fire (2011) and one year after (2012) using the Composite Burn Index (CBI) for explaining the post-fire vegetation response, which is measured using VHR satellite imagery. To determine this relationship, we applied redundancy analysis (RDA), which allowed us to identify which satellite variables among VHR spectral bands and Normalized Difference Vegetation Index (NDVI) can better express the post-fire vegetation response. Results demonstrated that in the first year after the fire event, variations in the post-fire vegetation dynamics can be properly detected using the GeoEye VHR data. Furthermore, results showed that remotely-sensed NDVI-based variables are able to encapsulate burn severity variability over time. Our analysis showed that, in this specific case, burn severity variations are mildly affected by the topography, while the NDVI index, as inferred from VHR data, can be successfully used to monitor the short-term post-fire dynamics of the vegetation recovery.

Keywords: burn severity; Composite Burn Index (CBI); post-fire dynamics; redundancy analysis

1. Introduction

Over the last decades, forest fires have become more frequent, prolonged, and severe than ever before [1,2], especially in the Mediterranean region. As such, fires have long-lasting and devastating impacts on forest ecosystems both in ecological and socio-economic terms. Therefore, it is now more important than ever to act upon enforcing sustainable fire management policies and promote forest sustainability [3].

To decide upon effective policies, national governments and stakeholders require accurate and detailed information regarding the impact of wildfires on forest ecosystems and their response after the disturbance [4–6]. Accurate information regarding the spatial distribution and level of damage (i.e., burn severity), as well as the post-fire vegetation recovery, is essential to quantify the impact of fire on the landscape, select and prioritize treatment measures, and plan and monitor restoration activities [7]. The overall effectiveness of post-fire management plans (restoration activities, etc.)

depends highly on understanding the relationships between patterns, dynamic processes, and potential restorative measures [3].

Such relationships are documented in the literature through the use of the term "burn severity". The burn severity metric is commonly defined in the literature as "a measure that gauges the magnitude of ecological change caused by fire and is related to short and long-term changes in vegetation structure and soil composition" [2,3,8,9]. The use of such a burn severity metric has been extensively studied in the past and it is now well understood that the good knowledge of the spatiotemporal variability of burn severity is key to understanding the vegetation response after a fire incident [10–13].

According to the literature, the time spans at which different plant species respond to burn severity may vary significantly [14]. Such differences in response timing have been shown to be one of the most critical factors that directly affects the post-fire succession in Mediterranean ecosystems [14]. Understanding the dominant time-scales at which burn severity influences vegetation the most, could improve our knowledge regarding the resilience of vegetation to fires [15].

Burn severity is controlled by many diverse biotic and abiotic parameters: vegetation type (fire sensitive species or fire adapted species), stand structure [16], topography (i.e., slope and aspect), and climatic conditions [9,17–21]. According to the study by Birch et al. [9] the two most important factors in controlling burn severity are vegetation cover and topography. Burn severity in forested areas has been shown to strongly depend on the dominant pre-fire tree species [17,18]. The magnitude of severity is usually very high in areas covered by flammable conifer species and medium or low in areas covered by less flammable species, such as broadleaves [22]. Topography is also an important factor that influences burn severity. In general, prior and after the fire event, topography plays a crucial role in many ecological processes, as it greatly affects the fire proneness of an area, as well as the post-fire vegetation dynamics [23,24]. However, the association among vegetation response, topography, and burn severity cannot be generalized for all ecosystems. Therefore, it is strongly recommended to the land managers to investigate the above relationship for each ecosystem separately, before making any important management decision [2].

Several methods have been proposed for measuring short and long-term burn severity. The Composite Burn Index (CBI) proposed by [25,26] is the most widely used field-based index for quantifying burn severity. CBI field measurements are usually coupled with medium-resolution satellite data like Landsat data (30 m), in order to map burn severity over large areas [27]. The level of fire damage in remote sensing studies is usually inferred from satellite images using indexes such as the Differenced Normalized Burn Ratio (dNBR) and the Normalized Difference Vegetation Index (NDVI) [13,28]. Examples of successful uses of CBI estimations along with satellite data can be found in [12,29–31].

Most research found in the literature about burn severity has been carried out using medium-resolution satellite data, as opposed to a handful of studies which evaluate burn severity from very-high-resolution (VHR) satellite data [27,31]. However, the thematic precision of these studies is generally insufficient for studying burn severity implications at a small scale. As a result, the production of burn severity maps, particularly at very high spatial resolutions, still remains an active research topic [32]. In general, burn severity studies require more detailed inventories. This is because more accurate information regarding the different levels of burn severity is expected to aid our understanding about the complex effects of fire [18].

The goal of generating accurate local-level burn severity map products is usually accomplished using VHR imagery, combined with one of the existing classification methods [7]. However, as new technology (e.g., new sensors) and advanced image analysis techniques becomes available, burn severity classifications will increasingly need to be adjusted in order to reflect any additional fire effects detected by new VHR sensors [32]. In this context, it is of paramount importance for the stakeholders to determine the degree of consistency between the burn severity field data and the VHR satellite data.

To date, however, there is a lack of studies examining the interrelationship between burn severity, ecosystem response, and topography, especially over the complete extent of a large fire [13,33–35].

This could be because such studies require extensive and costly field measurements for extracting the burn severity metric. Although VHR data have been mainly used for assessing burn severity, there remains a need to explore the interrelationships between remotely-sensed measurements and the physical/ecological processes that the CBI index infers [3].

So far, a limited number of studies have found statistical correlations between fire severity metrics, topography, VHR satellite data, and ecosystem responses [9,28,36,37]. This has generated the need for more studies focused on the understanding of these relationships.

The main objectives of this study are (i) to investigate the potential of the remotely-sensed post-fire vegetation response data as an expression of field-measured burn severity and topography; and (ii) to identify the best satellite variables (bands and NDVI index) able to capture the post-fire vegetation dynamics in the short-term. In this perspective this study used VHR GeoEye images of a forest fire that occurred in Evros (Greece) during summer 2011, in relationship with the CBI measured immediately after the fire (November 2011) and one year after the fire (August 2012).

2. Study Area

The study area is located in Evros, Greece's northernmost prefecture (40°57′–41°0′N and 26°2′–26°8′E) (Figure 1). Evros is located in the eastern-northeastern part of Thrace and shares international borders with Turkey to the east and Bulgaria to the north. The forests in this region are mainly composed of conifers, oaks, and beeches, and they are widely known for their unique ornithological and ecological value. The climate in this region is mainly Mediterranean, although it is affected by continental conditions.

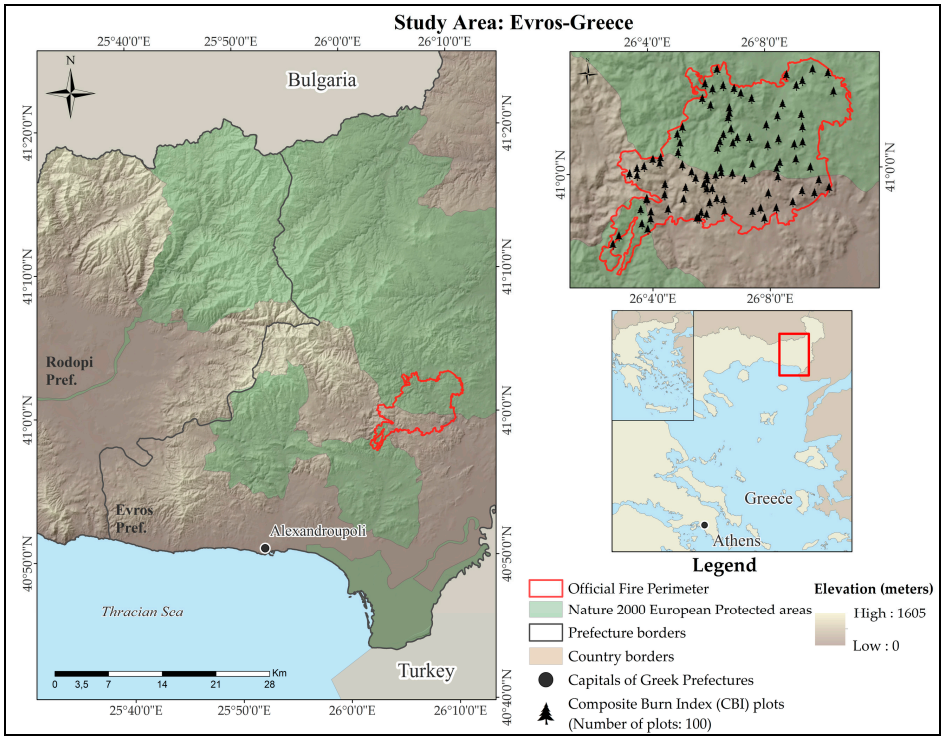

Figure 1. Location of the study area. The area delineated with red is the area of Evros (Greece) which was severely affected by a large fire in August 2011. The detail on the upper right depicts the locations which were visited in the field in order to measure the Composite Burn Index (CBI).

The area was affected by a large forest fire (5996 ha) in the summer of 2011. The fire started on 24 August 2011 and it was extinguished three days later, on 27 August 2011. Prior the the fire the area was mainly covered by coniferous (29.96%), oak (18.39%), and mixed oak–coniferous forests (27.15%).

The fire is the first fire event after the reforestation interventions that took place in the mid-1970s. The predominant types of landcover at that point of time (in the mid-1970s) was makia vegetation and sparse oak forests. The area's elevation varies from 0 m to 1650 m above sea level, whereas the elevation within the fire perimeter varies from 35 m to 433 m (Figure 2).

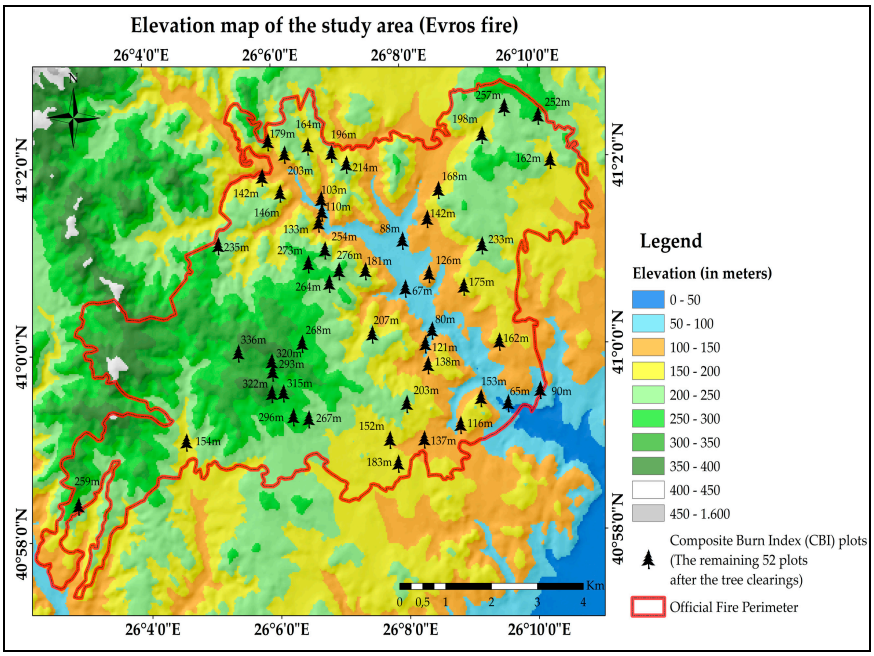

Figure 2. Elevation map and geographical position of the CBI plots (52) left after the tree clearings. The color scale illustrates values of elevation change. The black trees in the map, indicate the CBI plot locations.

3. Datasets and Preprocessing

3.1. Field Data

We collected two sets of data over 100 randomly-selected 60 × 60 m plots (Figure 1). The first set of data was collected in November 2011 immediately after the fire incident, and the second one a year later, in August 2012. To select the location of our burn severity data sampling, we used a stratified random sampling scheme based on a burn severity map. Such a map was derived using the object-based image analysis (OBIA) [38] method by classifying the multispectral four-band WorldView-2 imagery into seven classes: water, healthy vegetation, bare land/other land uses (ex.agricultural areas), high severity, high-medium severity, and medium-low severity.

The whole process was fulfilled in two main phases. In the first phase, we applied a multi-resolution segmentation to the WorldView-2 image. Throughout the procedure, we segmented the image and generated image objects based on several adjustable criteria of scale, band weights, and homogeneity in color and shape. Overall, we created two segmentation levels for the WorldView-2 image. In each level, the segmentation parameters were determined through a trial-and-error procedure. The first level targeted exclusively at agricultural areas by using the land-parcel identification system (LPIS) thematic layer parameter to segment the image. The LPIS thematic dataset is a vector layer that contains information about the boundaries of all Greek agricultural areas and it was used during the segmentation process to separate the agricultural areas from its surroundings. At the second level, the area outside the LPIS boundaries was segmented again in order to derive homogeneous objects that are representative of all of the remaining classes. In the second phase, we developed a rule-based classification model to classify image objects into the burn severity classes. In our analysis, the representative features of the object classes were determined with the

associated threshold value and implemented in the classification model. We regulated the membership of objects in certain classes via classification rules with fixed threshold values. Overall, the whole process resulted in the production of the previously-mentioned burn severity map.

The 100 CBI plots, which we selected based on the object-based burn-severity map, were positioned in the field by taking into account accessibility constraints. All CBI plots were located at least 100 m away from each other. Unfortunately, the Greek forest services, in an effort to aid the recovery of the ecosystem, allowed loggers to remove all of the dead trees and clear the burnt land. Due to this, we were able to use only 52 out of the initial 100 plots in our analysis.

To gauge the magnitude of ecological change caused by fire in the field, we adopted the Composite Burn Index (CBI). The CBI was measured for each plot, using an adapted version of the FIREMON landscape assessment methodology [1,8]. Burn severity was recorded using the FIREMON field form [8] and field digital photography. Five burn severity factors were visually assessed for each vegetation strata ((i) substrates; (ii) grasses, herbs, and small shrubs below 1 m; (iii) tall shrubs and trees up to 5 m; (iv) trees from 5 to 20 m; and (v) large trees taller than 20 m) within each plot, and were given a score ranging from zero to three (unburned to highest severity) [39]. In the following, a total CBI score was calculated for each plot by averaging the five rating factors measured in field. Finally, for the purposes of the statistical analysis, the CBI values were linearly scaled to the range between 0 and 1.

To provide additional information regarding the statistical attributes of the derived CBI variables (Time1CBI and Time2CBI) we plotted their histograms in Figure 3. From the figure we can see that in both examined cases (Time1 at 2011 and Time2 at 2012), the CBI scores are highly clustered around the high values (and, therefore, they are not very dispersed). This indicates that most of the plots have high CBI scores and implies that most of the areas examined in the field have been severely affected by the fire. Visual analysis of the two histograms indicates that there is a significant difference between the two distributions. In the case of the first histogram (Figure 3a) the majority of the CBI plots have high scores that fall into the 2.75–3 class whereas, in the second histogram, the number of plots that belong to this class has decreased significantly. In the first case examined (Time1CBI), the concentration of the CBI scores around the high values can be attributed to the fact that, immediately after the fire, the effects of burn severity were very intense. This find also agrees with our field observations. In the second case (Time2CBI) (Figure 3b) the fact that the number of CBI plots with the highest scores is decreased can be explained by the fact that one year after the fire the ecosystem has started recovering.

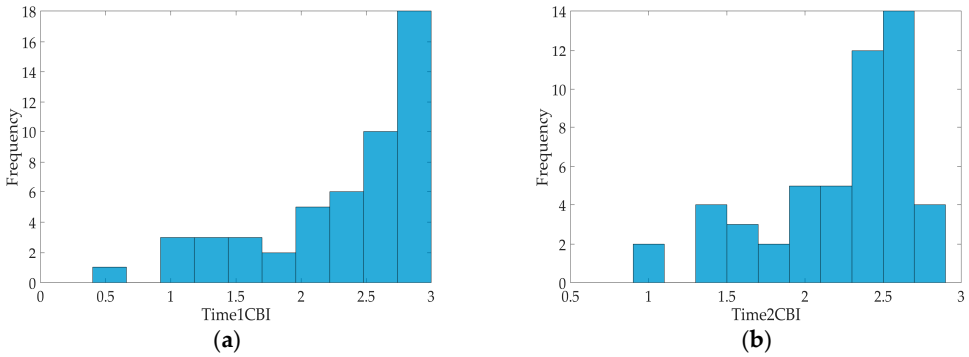

Figure 3. Distributions of mean CBI values for (**a**) Time1 (2011) and (**b**) Time2 (2012).

3.2. Satellite Data

Two satellite images collected by the GeoEye sensor (2 m) were used for the statistical analysis (Table 1). The first image was captured immediately after the fire (20 November 2011) and the second image was captured one year later (23 August 2012). Henceforth, the preprocessed images will be referred, respectively, as $\text{GeoEye}_{\text{time1}}$ and $\text{GeoEye}_{\text{time2}}$.

The two GeoEye images were atmospherically corrected, using the ATCOR 2 software (Wessling, Germany), and ortho-rectified with the help of the 5 m Digital Elevation Model [40]. The total RMS errors associated with the ground control points (GCPs) did not exceed 0.5 pixels in either of the two images. Auxiliary data, such as the Land-parcel Identification system (LPIS) data for Greece and a WorldView-2 image captured soon after the fire event, were also used during the object-based classification process.

To investigate the relationship between the VHR satellite data (GeoEye) and the field-measured burn severity, for each CBI plot we identified a 60 m × 60 m area centered on each CBI field point, where we computed five remotely-sensed variables. First, we computed the mean value of each spectral band (i.e., blue, green, red, near-infrared). Then, since various studies have shown that the variation of the vegetation cover after a severe fire event is highly correlated with the magnitude of the burn severity [12,33,41] we computed the mean Normalized Difference Vegetation Index (NDVI) [42] per sampling plot. We applied the same procedure to both post-fire images (i.e., $\text{GeoEye}_{\text{time1}}$ and $\text{GeoEye}_{\text{time2}}$). Overall, we derived 10 variables. Figure 4 presents the histograms of the derived variables. From the figure we can see that variation exists in all variables. Ultimately, all of the aforementioned variables were linearly scaled to the range (0, 1) [7]. For better understanding of the NDVI variable, Figure 5 presents the variability within the CBI plots of different levels of burn severity.

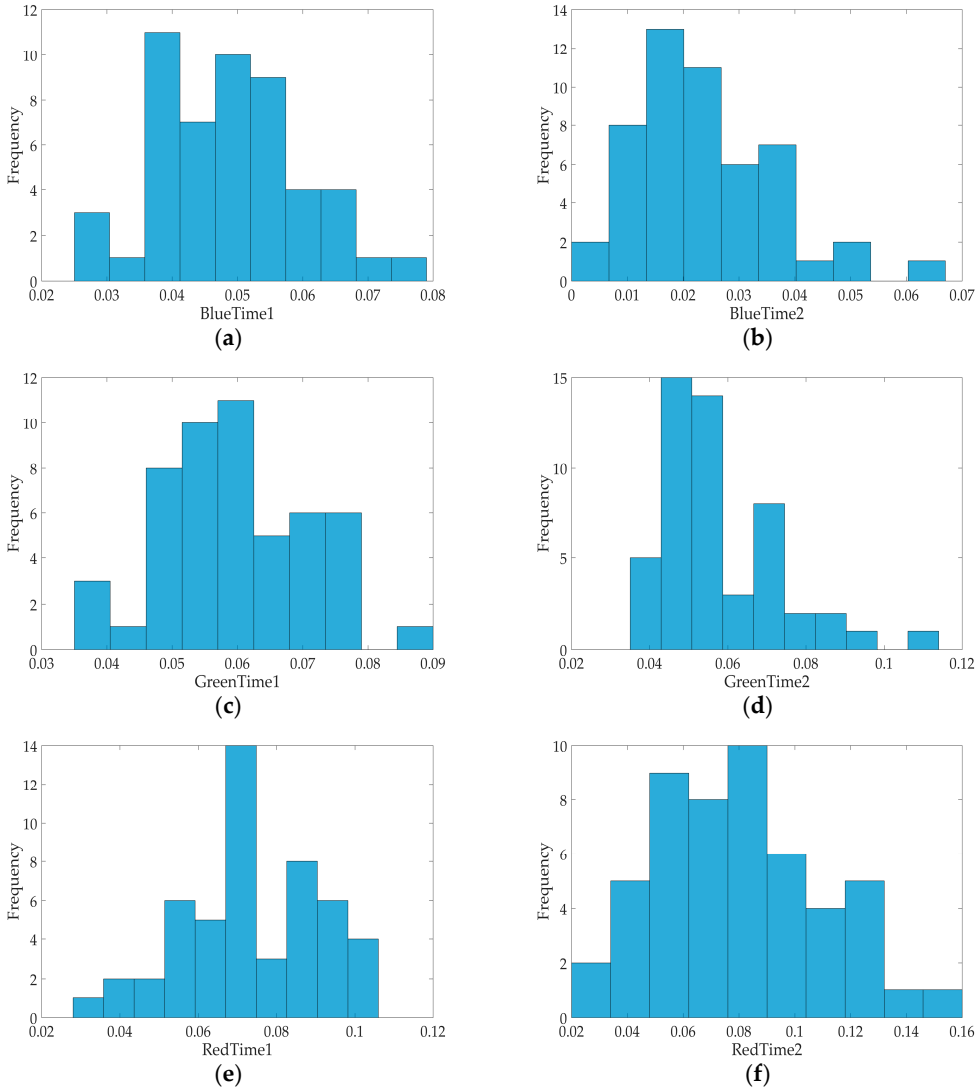

Figure 4. *Cont.*

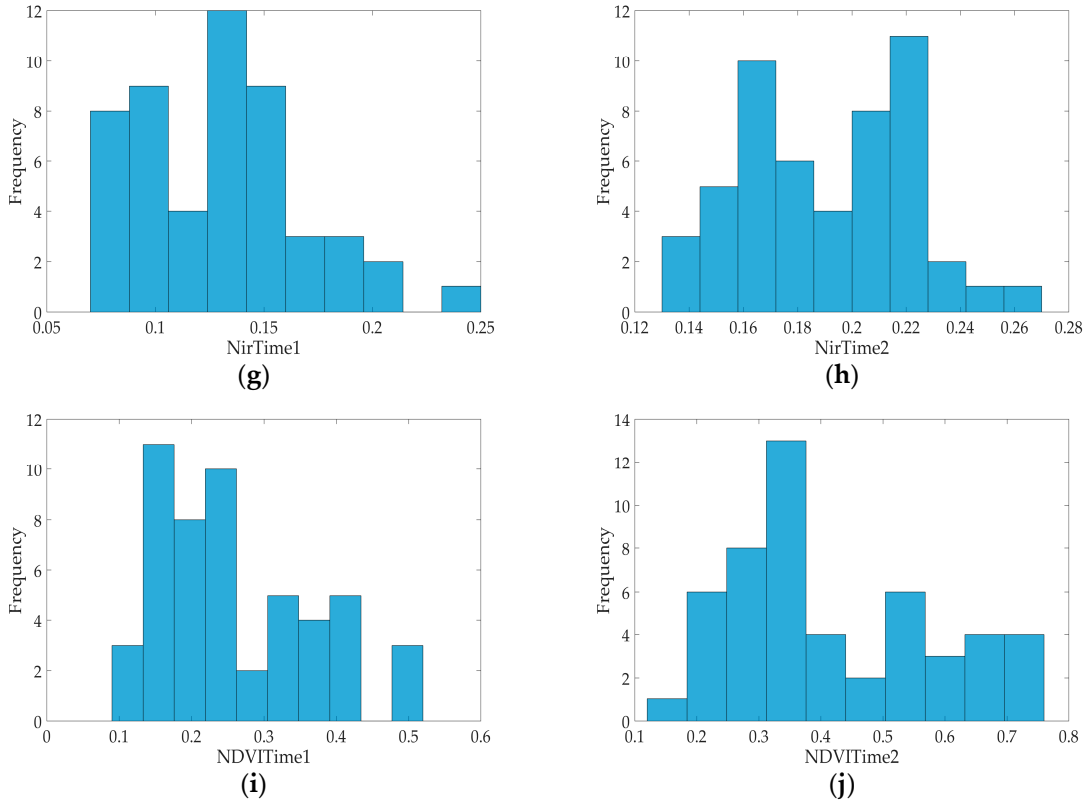

Figure 4. Histograms for the 10 satellite-derived variables. These distributions were obtained after plotting the mean values of the two sets of CBI plots, for each band and each different image (GeoEye 2011 and 2012); (**a**) blue band histogram for the year 2011; (**b**) blue band histogram for year 2012; (**c**) green band histogram for the year 2011; (**d**) green band histogram for the year 2012; (**e**) red band histogram for the year 2011; (**f**) red band histogram for the year 2012; (**g**) NIR band histogram for the year 2011; (**h**) NIR band histogram for the year 2012; (**i**) NDVI band histogram for the year 2011; and (**j**) NDVI band histogram for the year 2011.

In this study we used the NDVI index as a proxy for quantifying the magnitude of post-fire vegetation response in GeoEye images (Equation (1)):

$$NDVI = \frac{NIR_{band} - RED_{band}}{NIR_{band} + RED_{band}} \quad (1)$$

NDVI is a commonly used index for post-fire vegetation response in the literature [2,33,43] and is based on the absorption and reflection characteristics of plants in the red and near-infrared spectral regions [12]. In addition to NDVI, previous work [44] has proposed the use of the Normalized Burn Ratio (NBR) [26], and the differenced Normalized Burn Ratio (dNBR) [26] for detecting and monitoring post-fire vegetation changes over time. Unfortunately, their use was not possible in this study because they require data from regions of the optical spectrum that are not available in GeoEye images (Table 1). More specifically, the NBR index requires multispectral sensors with a NIR band between 0.76–0.9 μm and a SWIR band between 2.08–2.35 μm.

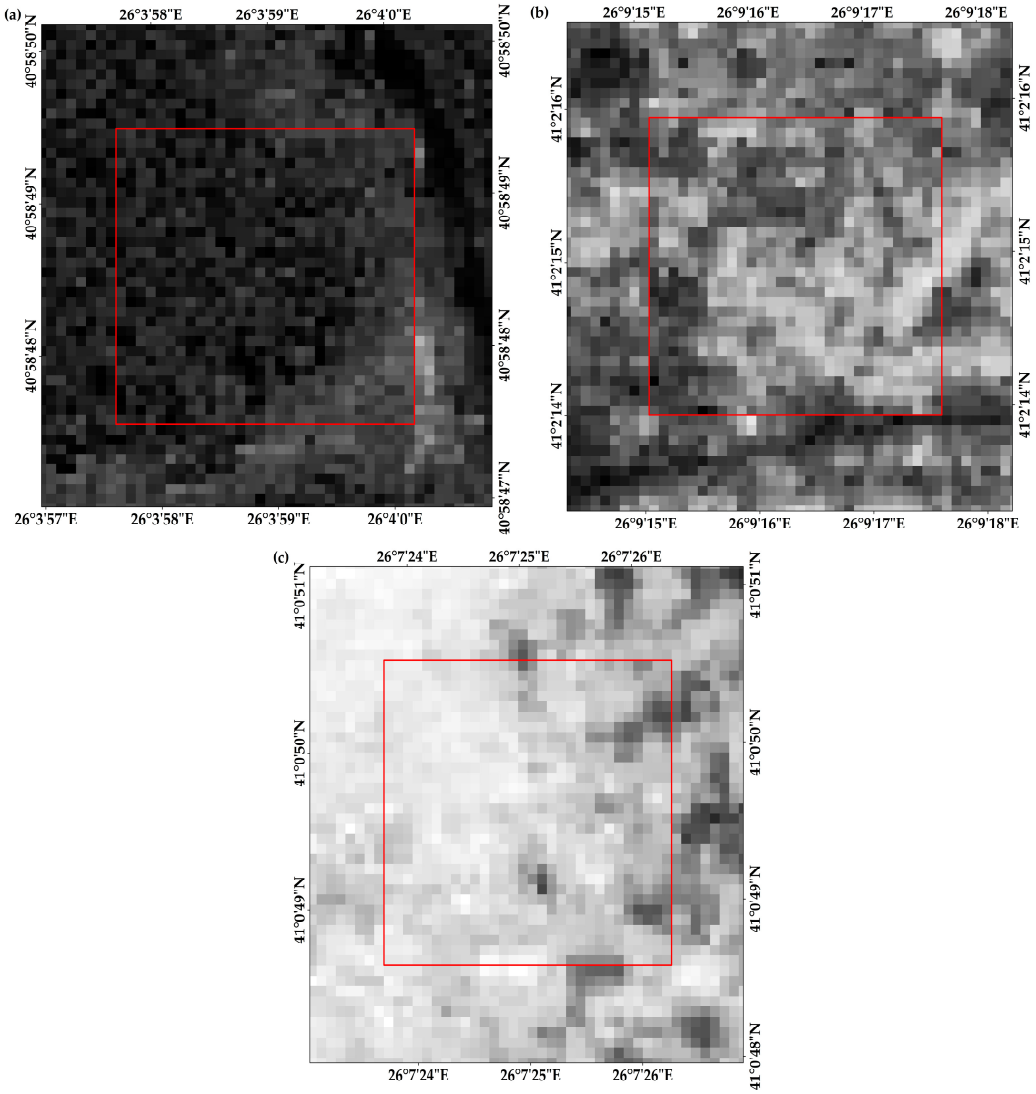

Figure 5. Visual representation of the NDVI variability in three different burn severity field plots. The areas delineated with red are the 60 m × 60 m CBI field plots. (**a**) NDVI values within a high-severity CBI plot; (**b**) NDVI values within a moderate-severity CBI plot; and (**c**) NDVI values within a low-severity CBI plot. The background of the figure is the 2011 NDVI image.

Table 1. Characteristics of the satellite data used in this study.

Satellite Sensor	Code Name	Acquisition Date	Spectral Range
GeoEye-1	$GeoEye_{time1}$	20 November 2011	Blue: 450–510 nm Green: 510–580 nm Red: 655–690 nm Near Infra Red: 780–920 nm
GeoEye-1	$GeoEye_{time2}$	23 August 2012	Blue: 450–510 nm Green: 510–580 nm Red: 655–690 nm Near Infra Red: 780–920 nm
WorldView-2	-	Soon after the fire	Blue: 450–510 nm Green: 510–580 nm Red: 630–690 nm Near Infra Red 1: 770–895 nm

3.3. Topographic Data

We used a five-meter (5 m) DEM [40] to derive three topographic parameters: (a) aspect; (b) slope; and (c) elevation. The produced grids of aspect and slope were calculated in radians, while the elevation in meters. Aspect is a variable measured in circular scale, with values ranging from 0° to 360° degrees. The fact that angles 0° and 360° are identical in this scale imposes the conversion of aspect values into sine and cosine values [45]. As a result, the aspect values were initially converted from degrees to radians and then to sine and cosine values using ArcMap Raster Calculator. The converted aspect sine values ranged from −1 (at due west) to 1 (at due east) [46], while cosine values ranged from −1 (at due south) to 1 (at due north) [45].

The values of all the topographic parameters (aspect cosine, aspect sine, slope, and elevation) were obtained for all CBI sampling points by computing the mean of each variable within a window of 12 pixels × 12 pixels (60 m × 60 m plot area). Figure 6 presents the histograms of the derived variables. From the figure we can see that variation exists in all four variables. This implies that the CBI plots were collected from areas with diverse topographic characteristics. Finally, the values of these variables were linearly scaled between 0 and 1 in order to facilitate the statistical analysis.

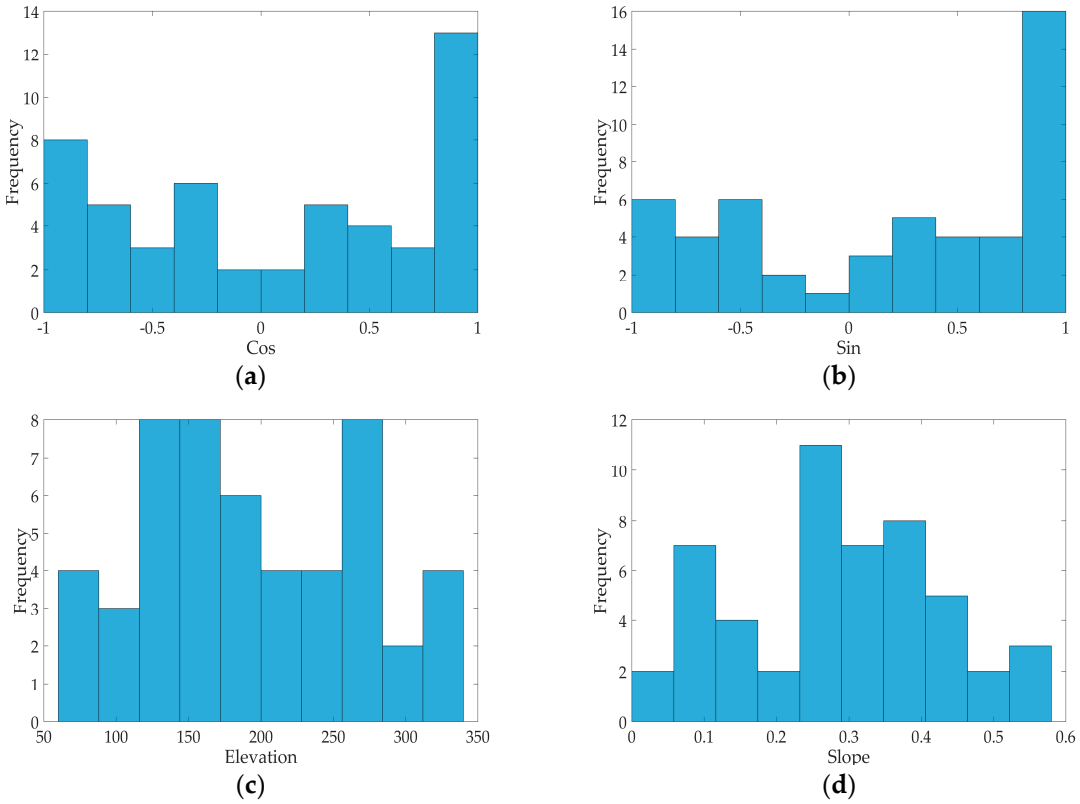

Figure 6. The topographic variables histograms of the CBI plots. (**a**,**b**) (from left to right) histograms for the mean cos and sin values of the CBI plots; and (**c**,**d**) histograms for the mean elevation and slope values of the CBI plots.

4. Methodology

To quantify the potential of VHR GeoEye satellite data to express the variations in the field-measured burn severity we used redundancy analysis (RDA) [47]. The RDA method was first developed by Rao [48,49]. RDA is a form of asymmetric canonical ordination technique widely used by ecologist and palaeoecologists [50]. The term "asymmetric" means that the two data matrices used in the analysis do not play the same role: there is a matrix of response variables, denoted Y, which often contains community composition data, and a matrix of explanatory variables (also referred to as

predictors) (e.g., environmental), denoted X, which is used to explain the variation in Y, as in regression analysis [49]. In this case, the term "redundancy" has a specific meaning and is used interchangeably with explained variance [49,51]. RDA can also be considered as an extension of principal component analysis because the ordination axes are linear combinations of the response variables (Y), but they are also constrained to be a linear function of the predictor [49]. Accordingly, the ordination of the dependent variables is forced to be explained by the configuration of the independent variables such that the RDA axes represent the percentage of the variance of the response variables explained by the predictors [52,53]. In a RDA biplot, the correlation among variables is given by the cosine of the angle between two vectors. Vectors pointing in roughly the same direction indicate a high positive correlation, vectors crossing at right angles correspond to a near zero correlation, and vectors pointing in opposite directions show a high negative correlation [54]. Environmental variables with long vectors are the most important in the analysis [55].

In order to identify the explanatory power of field-measured burn severity and topography on the vegetation post-fire response, we carried out the RDA using the topographic and CBI data as predictor variables (X), while the remotely-sensed VHR variables represented the response variables (Y). The rationale was to see if, through time, the satellite-based data can somehow express the field-measured burn severity and to quantify to what extent, in our study case, burn severity rather than topography influences the satellite-based data. RDA was performed using XLSTAT statistical software. We tested the significance of the analysis by running 500 permutations.

5. Results

The results obtained by applying the RDA method are presented in Figure 7 and Tables 2 and 3. Figure 6 illustrates that the first, second. and third axis represented, respectively, 95.83%, 2.81%, and 1.10% of the total variation of the multivariate system (p-value < 0.001); the first axis is, hence, the component which accounts for nearly the totality of the system variation.

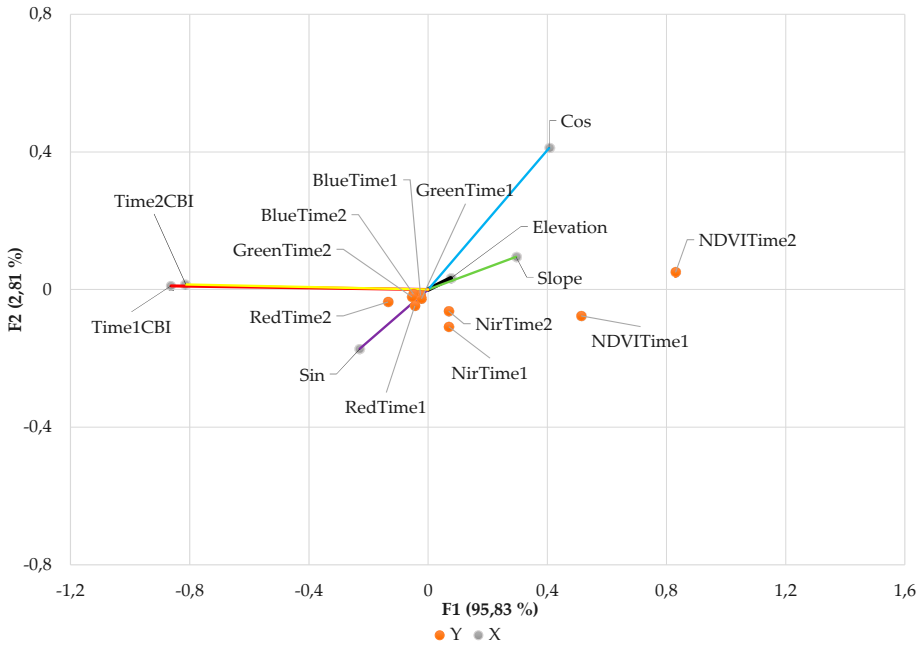

Figure 7. RDA biplot showing the explanatory variables (X) with lines (different color for each variable) and the response variables with orange dots.The RDA ordination plot was performed using the topographic (slope, aspect ,elevation) and field-measured CBI data as explanatory variables, and the remotely-sensed variables as response variables. The percent of the total variation that is explained by the first two canonical axes (F1 and F2) are 95.83% and 2.81%, respectively.

Table 2. RDA explanatory variables scores for the first three axis.

Variable	F1	F2	F3
Elevation	0.0764	0.0328	−0.4437
Slope	0.2954	0.0949	0.0787
Cos	0.4058	0.4115	−0.0962
Sin	−0.2299	−0.1725	−0.2778
Time1CBI	−0.8628	0.0109	0.0380
Time2CBI	−0.8127	0.0147	0.0127

Table 3. RDA response variables scores for the first three axis.

Variable	F1	F2	F3
BlueTime1	−0.0254	−0.0168	0.0269
GreenTime1	−0.0224	−0.0270	0.0272
RedTime1	−0.0445	−0.0474	0.0301
NirTime1	0.0691	−0.1078	0.0256
BlueTime2	−0.0495	−0.0128	0.0090
GreenTime2	−0.0542	−0.0216	0.0096
RedTime2	−0.1344	−0.0360	0.0078
NirTime2	0.0693	−0.0629	0.0287
NDVITime1	0.5136	−0.0763	−0.0722
NDVITime2	0.8301	0.0497	0.0457

According to Table 2, the most contributing variables to the first axis are the CBI ones at both times of measurement (Time1CBI and Time2CBI), while the topographic data are the least contributing variables. The response variables were mostly explained by the predictors NDVITime1 and NDVITime2 (Table 3); to the contrary the raw spectral data are only partially related to the considered explanatory variables.

6. Discussion

Burn severity is commonly defined as a measure of the magnitude of the short- to long-term ecological changes caused by fire [9]. Due to the challenges faced by resource managers in maintaining post-fire ecosystem health, there is a need for methods to assess the ecological consequences of disturbances and to monitor the vegetation changes occurring after a burning event [7].

Generally, topography plays an important role in vegetation dynamics prior and after the fire. Prior to the fire, topography influences the microclimate (temperature, precipitation, and direct solar radiation), plant productivity, and biomass accumulation that directly affects the amount of biomass available to burn during the outbreak of fire [18]. After the fire event, the topographic variations in slope, aspect, and elevation influences the microclimate at a local scale which, in turn, affects the post-fire regeneration rates [47].

Our statistical analysis results indicate that the two NDVI time variables are slightly correlated with slope, aspect, and elevation. This important finding can be attributed to two possible reasons. First, since the vegetation response to fire depends on many factors, it is likely that various factors other than the topography have an important influence on the post-fire vegetation response. Second, prior to the fire the studied area was mainly covered by *Pinus* reforestations, all of which were established on areas with similar altitudes. For this reason a large number of samples (CBI field measurements) were selected from areas with similar altitude. The fact that the statistical analysis is based on a dataset with samples taken from similar altitudes may explain the lack of elevation influence on the post-fire vegetation response. Even though these statements need further investigation in order to arrive to concrete conclusions, it is clear that the restoration planning can greatly benefit from insights into the vegetation response to local environmental conditions.

Following, the results showed that there is a high negative correlation between the two CBI time variables and the corresponding NDVI (NDVITime1 and NDVITime2). This negative correlation is attributed to the fact that during the course of time, the ecosystem responds to disturbance which, in turn, affects the degree of burn severity. That is, the increased satellite-derived NDVI values are associated with lower degree of burn severity in the field. Several studies have shown that the variation of the vegetation cover after a severe fire event is highly correlated with the magnitude of burn severity [7,12,33]. This indicates that the NDVI data extracted from the GeoEye imagery, was able to capture the ecosystem response to fire, which was quantified using the field-based CBI measurements.

The strong, negative correlation between the CBI and NDVI variables demonstrated that GeoEye images captured soon after the fire are capable of detecting the short term (up to one year) bi-temporal variations in burn severity. A possible explanation is that the fire effects are quite homogeneous and easy to measure short after the disturbance [18]. Even though in this study we focused on the short-term relationship between the GeoEye images and the fire effects, it would be beneficial to extend our analysis by looking at the long-term relationship. To do so, we will need a much larger dataset of field-measured burn severity that is not currently available. Extracting information from imagery with higher spectral, spatial, and temporal resolutions is expected to augment existing information regarding ecosystems response after fire.

In summary, the results of this study showed that satellite-derived NDVI time variables are highly associated with the CBI field-measured variables. This observation emphasizes the role of the VHR GeoEye remotely-sensed data in monitoring burn severity through space and time. This work is a preliminary study, in which the relationship between the field-measured CBI index and the VHR GeoEye satellite data are explored. To the best of our knowledge there is no burn severity index found in literature to be specifically designed for VHR satellite data. Hence, the results of this study could possibly provide a first guide for designing a new burn severity index specifically focused on VHR satellite data. Since the results of this study have the limit to be site specific, further research is needed to fully understand the interrelationships between topography, field measured burn severity, and the post-fire vegetation response, which, in this specific case, has been quantified using VHR GeoEye satellite data. In this context, it would be very interesting to examine how the previously-mentioned relationships vary over longer time spans and different study areas.

7. Conclusions

Fire and burn severity studies will continue to depend on satellite data and field-based burn severity data. As generally known, field sampling is very complicated due to several factors, like survey costs, the accessibility of the locations, the limited surface coverage, etc. Finding a direct correlation between in situ measurements and remotely-sensed data also in this research field may have useful implications in terms of post-fire analysis, recovery strategies, intervention and land management work. Therefore, it is to the best interest of stakeholders and local managers to improve the quality of the burn severity information. To do so, it is critical to associate the burn severity field measurements with the appropriate satellite image. The results of this study indicate, that short term burn severity can be successfully estimated using GeoEye images. Accurate burn severity estimates will augment existing information regarding the ecosystems response after fire. Furthermore, this kind of study can open new perspectives in terms of environmental applications of new sensor products.

Acknowledgments: This research work was conducted as part of the project "National Observatory of Forest Fires (NOFFi)" which is done in collaboration with the Greek Special Secretariat for Forests and financially supported by the Green Fund.

Author Contributions: Eleni Dragozi proposed the employed methodology and developed the research design, performed the experimental analysis, manuscript writing, and results interpretation. Ioannis Gitas and Sofia Bajocco contributed to the research design, results interpretation, discussion writing and manuscript revision. Dimitris Stavrakoudis contributed to the interpretation of the obtained results and manuscript writing.

Conflicts of Interest: The authors declare no conflict of interest.

References

1. Moreira, F.; Viedma, O.; Arianoutsou, M.; Curt, T.; Koutsias, N.; Rigolot, E.; Barbati, A.; Corona, P.; Vaz, P.; Xanthopoulos, G. Landscape-wildfire interactions in southern Europe: Implications for landscape management. *J. Environ. Manag.* **2011**, *92*, 2389–2402. [CrossRef] [PubMed]
2. Hoscilo, A.; Tansey, K.J.; Page, S.E. Post-fire vegetation response as a proxy to quantify the magnitude of burn severity in tropical peatland. *Int. J. Remote Sens.* **2013**, *34*, 412–433. [CrossRef]
3. Lentile, L.B.; Holden, Z.A.; Smith, A.M.; Falkowski, M.J.; Hudak, A.T.; Morgan, P.; Lewis, S.A.; Gessler, P.E.; Benson, N.C. Remote sensing techniques to assess active fire characteristics and post-fire effects. *Int. J. Wildland Fire* **2006**, *15*, 319–345. [CrossRef]
4. Gouveia, C.; DaCamara, C.; Trigo, R. Post-fire vegetation recovery in Portugal based on spot/vegetation data. *Nat. Hazards Earth Syst. Sci.* **2010**, *10*, 673–684. [CrossRef]
5. Chen, X.; Vogelmann, J.E.; Rollins, M.; Ohlen, D.; Key, C.H.; Yang, L.; Huang, C.; Shi, H. Detecting post-fire burn severity and vegetation recovery using multitemporal remote sensing spectral indices and field-collected composite burn index data in a ponderosa pine forest. *Int. J. Remote Sens.* **2011**, *32*, 7905–7927. [CrossRef]
6. FAO. *State of the World's Forests-2014*; FAO: Rome, Italy, 2014.
7. Gitas, I.; Polychronaki, A.; Mitri, G.; Veraverbeke, S. *Advances in Remote Sensing of Post-Fire Vegetation Recovery Monitoring—A Review*; InTech: Vienna, Austria, 2012.
8. Key, C.H.; Benson, N.C. Landscape assessment (LA). *FIREMON: Fire Effects Monitoring and Inventory System*; General Technical Report RMRS-GTR-164-CD. Rocky Mountain Research Station, US Department of Agriculture, Forest Service: Fort Collins, CO, USA, 2006; pp. LA-1–LA-51.
9. Birch, D.S.; Morgan, P.; Kolden, C.A.; Abatzoglou, J.T.; Dillon, G.K.; Hudak, A.T.; Smith, A.M. Vegetation, topography and daily weather influenced burn severity in central Idaho and western Montana forests. *Ecosphere* **2015**, *6*, 1–23. [CrossRef]
10. Naveh, Z. Mediterranean uplands as anthropogenic perturbation dependent systems and their dynamic conservation management. In *Terrestrial and Aquatic Ecosystems, Perturbation and Recovery*; Ellis Horwood: New York, NY, USA, 1991; pp. 544–556.
11. Ryan, K.C. Dynamic interactions between forest structure and fire behavior in boreal ecosystems. *Silva Fenn.* **2002**, *36*, 13–39. [CrossRef]
12. Schepers, L.; Haest, B.; Veraverbeke, S.; Spanhove, T.; Vanden Borre, J.; Goossens, R. Burned area detection and burn severity assessment of a heathland fire in Belgium using Airborne Imaging Spectroscopy (APEX). *Remote Sens.* **2014**, *6*, 1803–1826. [CrossRef]
13. Ireland, G.; Petropoulos, G.P. Exploring the relationships between post-fire vegetation regeneration dynamics, topography and burn severity: A case study from the Montane Cordillera Ecozones of Western Canada. *Appl. Geogr.* **2015**, *56*, 232–248. [CrossRef]
14. Catry, F.; Rego, F.; Moreira, F.; Fernandes, P.; Pausas, J. Post-fire tree mortality in mixed forests of central Portugal. *For. Ecol. Manag.* **2010**, *260*, 1184–1192. [CrossRef]
15. Driscoll, D.A.; Lindenmayer, D.B.; Bennett, A.F.; Bode, M.; Bradstock, R.A.; Cary, G.J.; Clarke, M.F.; Dexter, N.; Fensham, R.; Friend, G. Fire management for biodiversity conservation: Key research questions and our capacity to answer them. *Biol. Conserv.* **2010**, *143*, 1928–1939. [CrossRef]
16. Moreira, F.; Arianoutsou, M.; Vallejo, V.R.; de las Heras, J.; Corona, P.; Xanthopoulos, G.; Fernandes, P.; Papageorgiou, K. Setting the scene for post-fire management. In *Post-Fire Management and Restoration of Southern European Forests*; Springer: Berlin, Germany; Heidelberg, Germany, 2012; pp. 1–19.
17. Viedma, O.; Quesada, J.; Torres, I.; De Santis, A.; Moreno, J.M. Fire severity in a large fire in a Pinus pinaster forest is highly predictable from burning conditions, stand structure, and topography. *Ecosystems* **2014**, *18*, 237–250. [CrossRef]
18. Morgan, P.; Keane, R.E.; Dillon, G.K.; Jain, T.B.; Hudak, A.T.; Karau, E.C.; Sikkink, P.G.; Holden, Z.A.; Strand, E.K. Challenges of assessing fire and burn severity using field measures, remote sensing and modelling. *Int. J. Wildland Fire* **2014**, *23*, 1045–1060. [CrossRef]

19. Karaman, M.; Özelkan, E.; Örmeci, C. Determination of the forest fire potential by using remote sensing and geographical information system, case study-Bodrum/Turkey. In *Advances in Remote Sensing and GIS Applications in Forest Fire Management From Local to Global Assessments*; Publications office of the European Union: Stressa, Italy, 2011; pp. 51–55.
20. Collins, B.M.; Kelly, M.; van Wagtendonk, J.W.; Stephens, S.L. Spatial patterns of large natural fires in Sierra Nevada wilderness areas. *Landsc. Ecol.* **2007**, *22*, 545–557. [CrossRef]
21. Turner, M.G.; Hargrove, W.W.; Gardner, R.H.; Romme, W.H. Effects of fire on landscape heterogeneity in Yellowstone National Park, Wyoming. *J. Veg. Sci.* **1994**, 731–742. [CrossRef]
22. Pinto, A.; Fernandes, P.M. Microclimate and modeled fire behavior differ between adjacent forest types in Northern Portugal. *Forests* **2014**, *5*, 2490–2504. [CrossRef]
23. Boiffin, J.; Aubin, I.; Munson, A.D. Ecological controls on post-fire vegetation assembly at multiple spatial scales in eastern North American boreal forests. *J. Veg. Sci.* **2014**. [CrossRef]
24. Mouillot, F.; Ratte, J.-P.; Joffre, R.; Mouillot, D.; Rambal, S. Long-term forest dynamic after land abandonment in a fire prone Mediterranean landscape (central Corsica, France). *Landsc. Ecol.* **2005**, *20*, 101–112. [CrossRef]
25. Key, C.; Benson, N. Measuring and remote sensing of burn severity. In Proceedings of the Joint Fire Science Conference and Workshop, Boise, Idaho, 15–17 June 1999; p. 284.
26. Key, C.; Benson, N. *FIREMON: Fire Effects Monitoring and Inventory System*; USDA Forest Service, Rocky Mountain Research Station: Fort Collins, CO, USA, 2006.
27. Chuvieco, E. *Earth Observation of Wildland Fires in Mediterranean Ecosystems*; Springer: Berlin/Heidelberg, Germany, 2009.
28. Keeley, J.E. Fire intensity, fire severity and burn severity: A brief review and suggested usage. *Int. J. Wildland Fire* **2009**, *18*, 116–126. [CrossRef]
29. Mitri, G.H.; Gitas, I.Z. Mapping the severity of fire using object-based classification of IKONOS imagery. *Int. J. Wildland Fire* **2008**, *17*, 431–442. [CrossRef]
30. Amato, V.J.; Lightfoot, D.; Stropki, C.; Pease, M. Relationships between tree stand density and burn severity as measured by the Composite Burn Index following a ponderosa pine forest wildfire in the American Southwest. *For. Ecol. Manag.* **2013**, *302*, 71–84. [CrossRef]
31. Chen, G.; Metz, M.R.; Rizzo, D.M.; Dillon, W.W.; Meentemeyer, R.K. Object-based assessment of burn severity in diseased forests using high-spatial and high-spectral resolution MASTER airborne imagery. *ISPRS J. Photogramm. Remote Sens.* **2015**, *102*, 38–47. [CrossRef]
32. Keane, R.E.; Dillon, G.; Jain, T.; Hudak, A.; Morgan, P.; Karau, E.; Sikkink, P.; Silverstein, R. *The Problems with Fire Severity and Its Application in Fire Management*; USDA Forest Service, Rocky Mountain Research Station: Missoula, MT, Canada, 2012.
33. Díaz-Delgado, R.; Lloret, F.; Pons, X. Influence of fire severity on plant regeneration by means of remote sensing imagery. *Int. J. Remote Sens.* **2003**, *24*, 1751–1763. [CrossRef]
34. Edwards, A.C.; Maier, S.W.; Hutley, L.B.; Williams, R.J.; Russell-Smith, J. Spectral analysis of fire severity in north Australian tropical savannas. *Remote Sens. Environ.* **2013**, *136*, 56–65. [CrossRef]
35. Dzwonko, Z.; Loster, S.; Gawroński, S. Impact of fire severity on soil properties and the development of tree and shrub species in a Scots pine moist forest site in southern Poland. *For. Ecol. Manag.* **2015**, *342*, 56–63. [CrossRef]
36. Wang, G.G.; Kemball, K.J. The effect of fire severity on early development of understory vegetation following a stand-replacing wildfire. In Proceedings of the 5th Symposium on Fire and Forest Meteorology Jointly with 2nd International Wildland Fire Ecology and Fire Management Congress, Orlando, FL, USA, 16–20 November 2003; pp. 16–20.
37. Johnstone, J.F.; Chapin, F.S., III. Effects of soil burn severity on post-fire tree recruitment in boreal forest. *Ecosystems* **2006**, *9*, 14–31. [CrossRef]
38. Blaschke, T.; Hay, G.J.; Kelly, M.; Lang, S.; Hofmann, P.; Addink, E.; Feitosa, R.Q.; van der Meer, F.; van der Werff, H.; van Coillie, F. Geographic object-based image analysis—Towards a new paradigm. *ISPRS J. Photogramm. Remote Sens.* **2014**, *87*, 180–191. [CrossRef] [PubMed]
39. Cansler, C.A.; McKenzie, D. How robust are burn severity indices when applied in a new region? Evaluation of alternate field-based and remote-sensing methods. *Remote Sens.* **2012**, *4*, 456–483. [CrossRef]
40. Demirel, N.; Emil, M.K.; Duzgun, H.S. Surface coal mine area monitoring using multi-temporal high-resolution satellite imagery. *Int. J. Coal Geol.* **2011**, *86*, 3–11. [CrossRef]

41. Epting, J.; Verbyla, D. Landscape-level interactions of prefire vegetation, burn severity, and postfire vegetation over a 16-year period in interior Alaska. *Can. J. For. Res.* **2005**, *35*, 1367–1377. [CrossRef]
42. Tucker, C.J. Red and photographic infrared linear combinations for monitoring vegetation. *Remote Sens. Environ.* **1979**, *8*, 127–150. [CrossRef]
43. Casady, G.M.; van Leeuwen, W.J.; Marsh, S.E. Evaluating post-wildfire vegetation regeneration as a response to multiple environmental determinants. *Environ. Model. Assess.* **2010**, *15*, 295–307. [CrossRef]
44. Wu, Z.; Middleton, B.; Hetzler, R.; Vogel, J.; Dye, D. Vegetation burn severity mapping using Landsat-8 and WorldView-2. *Photogramm. Eng. Remote Sens.* **2015**, *81*, 143–154. [CrossRef]
45. Deng, Y.; Goodchild, M.F.; Chen, X. Using NDVI to define thermal south in several mountainous landscapes of California. *Comput. Geosci.* **2009**, *35*, 327–336. [CrossRef]
46. Wimberly, M.C.; Reilly, M.J. Assessment of fire severity and species diversity in the southern Appalachians using Landsat TM and ETM+ imagery. *Remote Sens. Environ.* **2007**, *108*, 189–197. [CrossRef]
47. Dillon, G.K.; Holden, Z.A.; Morgan, P.; Crimmins, M.A.; Heyerdahl, E.K.; Luce, C.H. Both topography and climate affected forest and woodland burn severity in two regions of the western US, 1984 to 2006. *Ecosphere* **2011**, *2*, 1–33. [CrossRef]
48. Rao, C.R. The use and interpretation of principal component analysis in applied research. In *Sankhyā: The Indian Journal of Statistics, Series A*; Springer: Berlin, Germany; Heidelberg, Germany, 1964; pp. 329–358.
49. Legendre, P.; Legendre, L.F. *Numerical Ecology*; Elsevier: Amsterdam, The Netherlands, 2012.
50. Legendre, P.; Oksanen, J.; ter Braak, C.J. Testing the significance of canonical axes in redundancy analysis. *Methods Ecol. Evol.* **2011**, *2*, 269–277. [CrossRef]
51. Gittins, R. *Canonical Analysis: A Review with Applications in Ecology*; Springer: Berlin, Germany; Heidelberg, Germany, 1985.
52. Van den Brink, P.J.; ter Braak, C.J. Principal response curves: Analysis of time-dependent multivariate responses of biological community to stress. *Environ. Toxicol. Chem.* **1999**, *18*, 138–148. [CrossRef]
53. Bajocco, S.; Rosati, L.; Ricotta, C. Knowing fire incidence through fuel phenology: A remotely sensed approach. *Ecol. Model.* **2010**, *221*, 59–66. [CrossRef]
54. Ter Braak, C.J.; Prentice, I.C. A theory of gradient analysis. *Adv. Ecol. Res.* **1988**, *18*, 271–317.
55. Legendre, P.; Legendre, L. *Numerical Ecology*, 2nd ed.; Elsevier: Amsterdam, The Netherlands, 1998.